TRAF6 is an amplified oncogene bridging the RAS and NF-κB pathways in human lung cancer

Daniel T. Starczynowski,[1,2] William W. Lockwood,[1,2] Sophie Deléhouzée,[2] Raj Chari,[1,2] Joanna Wegrzyn,[1,2] Megan Fuller,[1] Ming-Sound Tsao,[3] Stephen Lam,[1] Adi F. Gazdar,[4] Wan L. Lam,[1,2] and Aly Karsan[1,2]

[1]British Columbia Cancer Agency, Vancouver, British Columbia, Canada. [2]Department of Pathology and Laboratory Medicine, University of British Columbia, Vancouver, British Columbia, Canada. [3]Ontario Cancer Institute, Princess Margaret Hospital, Toronto, Ontario, Canada. [4]UT Southwestern Medical Center, Dallas, Texas, USA.

Somatic mutations and copy number alterations (as a result of deletion or amplification of large portions of a chromosome) are major drivers of human lung cancers. Detailed analysis of lung cancer–associated chromosomal amplifications could identify novel oncogenes. By performing an integrative cytogenetic and gene expression analysis of non–small-cell lung cancer (NSCLC) and small-cell lung cancer (SCLC) cell lines and tumors, we report here the identification of a frequently recurring amplification at chromosome 11 band p13. Within this region, only TNF receptor–associated factor 6 (*TRAF6*) exhibited concomitant mRNA overexpression and gene amplification in lung cancers. Inhibition of *TRAF6* in human lung cancer cell lines suppressed NF-κB activation, anchorage-independent growth, and tumor formation. In these lung cancer cell lines, RAS required TRAF6 for its oncogenic capabilities. Furthermore, TRAF6 overexpression in NIH3T3 cells resulted in NF-κB activation, anchorage-independent growth, and tumor formation. Our findings show that TRAF6 is an oncogene that is important for RAS-mediated oncogenesis and provide a mechanistic explanation for the previously apparent importance of constitutive NF-κB activation in RAS-driven lung cancers.

Introduction

Characterization of the genome has revealed genes critical to the malignant landscape of human lung cancers. The 2 major forms of lung cancer are non–small-cell lung cancer (NSCLC) and small-cell lung cancer (SCLC). NSCLC represents the majority of all lung cancers at 85%, compared with 15% for SCLC (1). NSCLCs are histologically subdivided into squamous cell carcinoma, large-cell carcinoma, and adenocarcinoma. Somatic activating mutations of v-Ki-ras2 Kirsten rat sarcoma viral oncogene homolog (*KRAS*) are the most frequent genetic events in NSCLC, occurring in greater than 30% of cases (1). Despite the prominence of MAPK pathway activation by RAS, NF-κB also appears to be an essential pathway for *KRAS*-mediated NSCLC (2). The importance of NF-κB is further supported by reports of constitutive NF-κB activation in more than 50% of lung cancers (3). Despite high levels of NF-κB activation in lung tumors and a critical role in RAS-mediated lung cancer formation in vivo, the mechanisms leading to constitutive NF-κB are not known. Although *KRAS* mutations are rare in SCLC, activating mutations of the receptor tyrosine kinase mesenchymal-epithelial transition factor (*c-MET*) are among the most frequent in SCLC and thought to require the *KRAS* pathway for lung malignancies (4). Inactivating mutations of *TP53* are also common in NSCLCs (50%–80%) and SCLCs (80%–100%) (1).

In addition to somatic mutations, recurring cytogenetic alterations are also associated with lung cancers. Common deletions involving 5q11.2 (*PDE4D*), 7q11.22 (*AUTS2*), 9p21.3 (*CDKN2A* and *CDKN2B*), and 10q23.31 (*PTEN*) harbor known and candidate tumor suppressor genes (5). In contrast, recurring amplifications of 1q21.2 (*ARNT*), 5p15.3 (*TERT*), 7p11.2 (*EGFR*), 7q31.2 (*MET*), 8q24.21 (*MYC*), 11q13.3 (*CCND1*), 12p12.1 (*KRAS*), 14q13.3 (*NKX2-1*; also known as *TITF1*), and 17q12 (*ERBB2*) harbor known oncogenes (5, 6), implicating DNA amplifications as a mechanism of oncogene activation in lung cancers (7). In an attempt to identify novel oncogenes within lung cancer–associated amplicons, we performed a large-scale integrative cytogenetic and gene expression analysis of lung cancer cell lines and tumors. Here we report the identification of a frequently recurring amplification at chromosome 11p13. Examination of genes within the minimally amplified region on 11p13 revealed that TNF receptor–associated factor 6 (*TRAF6*) is a key candidate oncogene. Overexpression of TRAF6 in nontransformed cells resulted in NF-κB activation, anchorage-independent growth, and tumor formation. In contrast, inhibition of *TRAF6* in human lung cancer cells suppressed NF-κB activation, anchorage-independent growth, and tumor formation. Furthermore, RAS was dependent on TRAF6 for anchorage-independent growth and tumor formation. Therefore, the present study identifies *TRAF6* as a commonly amplified oncogene bridging RAS and NF-κB in lung cancer.

Results

High-resolution and whole-genome DNA platforms have allowed for reanalysis of tumor samples and identification of cryptic alterations. To identify novel genomic alterations in lung cancers, we used whole-genome tiling path array comparative genomic hybridization (aCGH) to determine copy number changes for 346 NSCLC and SCLC samples (85 cell lines and 261 primary tumors). Significance of recurrent gains or deletions was determined for the lung cancer cell lines using Genomic Identification of Significant Targets in Cancer (GISTIC), a statistical method that calculates

Conflict of interest: The authors have declared that no conflict of interest exists.
Citation for this article: *J Clin Invest.* 2011;121(10):4095–4105. doi:10.1172/JCI58818.

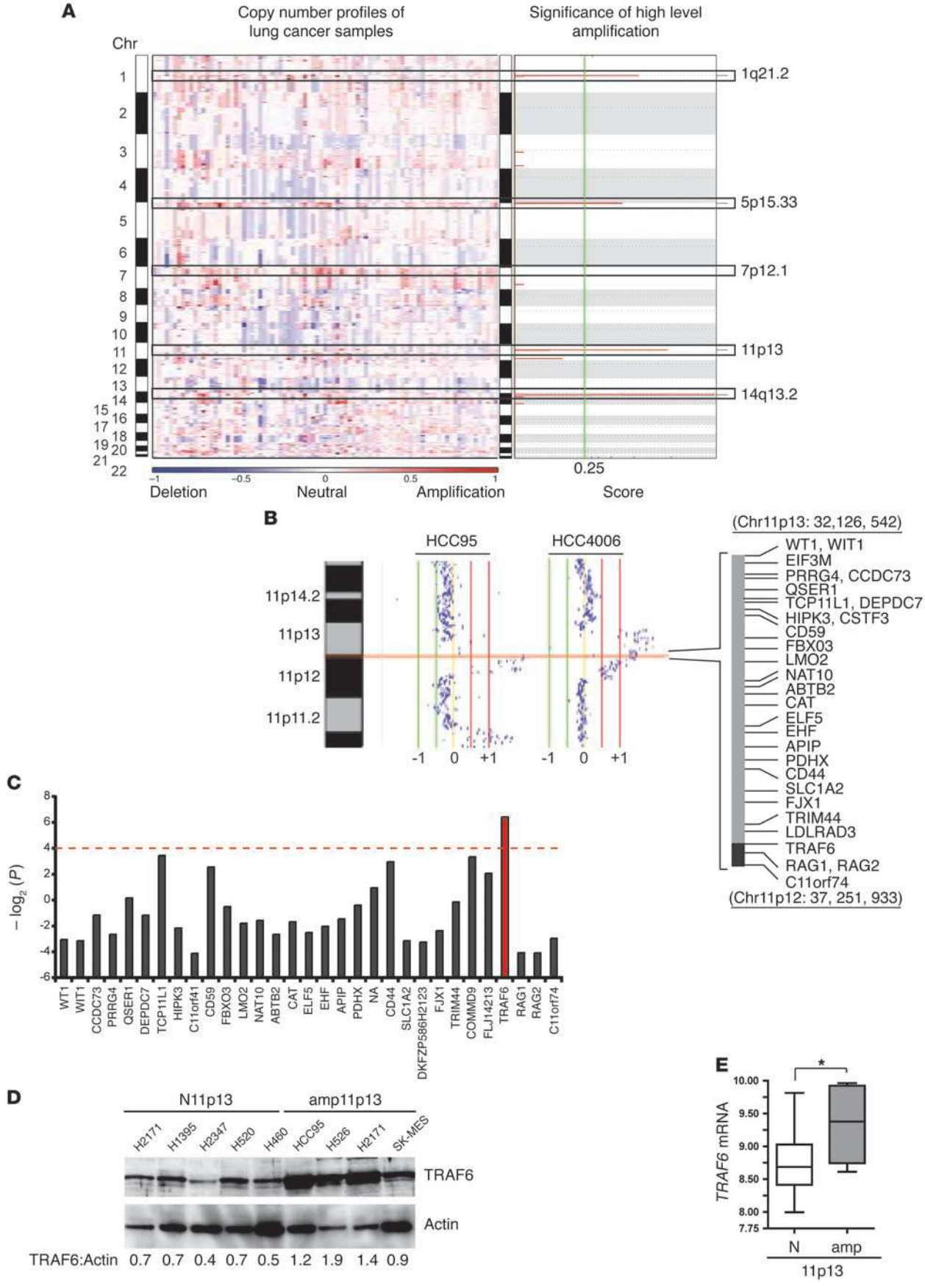
A
Copy number profiles of lung cancer samples
Significance of high level amplification
Chr
1q21.2
5p15.33
7p12.1
11p13
14q13.2
0.25
Deletion
Neutral
Amplification
Score
B
HCC95
HCC4006
11p14.2
11p13
11p12
11p11.2
(Chr11p13: 32,126, 542)
WT1, WIT1
EIF3M
PRRG4, CCDC73
QSER1
TCP11L1, DEPDC7
HIPK3, CSTF3
CD59
FBX03
LMO2
NAT10
ABTB2
CAT
ELF5
EHF
APIP
PDHX
CD44
SLC1A2
FJX1
TRIM44
LDLRAD3
TRAF6
RAG1, RAG2
C11orf74
(Chr11p12: 37, 251, 933)
C
– log2 (P)
WT1
WIT1
CCDC73
PRRG4
QSER1
DEPDC7
TCP11L1
HIPK3
C11orf41
CD59
FBXO3
LMO2
NAT10
ABTB2
CAT
ELF5
EHF
APIP
PDHX
NA
CD44
SLC1A2
DKFZP586H2123
FJX1
TRIM44
COMMD9
FLJ14213
TRAF6
RAG1
RAG2
C11orf74
D
N11p13
amp11p13
H2171
H1395
H2347
H520
H460
HCC95
H526
H2171
SK-MES
TRAF6
Actin
TRAF6:Actin 0.7 0.7 0.4 0.7 0.5 1.2 1.9 1.4 0.9
E
TRAF6 mRNA
N
amp
11p13

Figure 1
TRAF6 locus amplification occurs frequently in lung cancer. (**A**) Copy number data for 85 lung cancer lines is shown by genomic location (rows). False discovery rates (*q* values; 0.25 cutoff for significance shown by green line) and scores for amplicons are plotted at each genome position. Individual chromosomes are denoted by white and gray shading; black boxes indicate significant high-level amplifications. (**B**) Copy number status of chromosome 11p for 2 representative lung cancer lines. The minimally amplified region spanning chromosome 11p13 to 11p12 (32,126,542–37,251,933) and known genes are shown at right. Normalized $\log_2$ signal intensity ratios were plotted and visualized by SIGMA² (32). Vertical lines denote $\log_2$ signal ratios from –1 to +1; copy number gains (red) are to the right of 0. Each dot represents a single probe. (**C**) A subset of 66 lung cancer samples was analyzed to identify genes whose expression correlated with gene amplification. *P* values ($-\log_2$) for genes within the minimally amplified region on 11p13 are shown as a histogram. Values above the dashed line denote $P \leq 0.05$. (**D**) IB for TRAF6 and actin in 5 lung cancer lines diploid at 11p13 (N, no 11p13 amplification; H2171, H1395, H2347, H520, and H460) and 4 lung cancer lines with an 11p13 amplification (amp; HCC95, H526, H2171, and SK-MES-1). Densitometric values for TRAF6 protein relative to actin are shown below. (**E**) TRAF6 mRNA levels were evaluated in lung tumor samples with ($n = 13$) and without ($n = 31$) amplification of 11p13. Significance was determined by Mann-Whitney *U* test. $^*P < 0.05$.

significance scores incorporating the amplitude and frequency of copy number alterations at each position in the genome (8).

GISTIC analysis identified 5 significant high-level focal copy number amplifications ($\log_2$ ratio > 0.8) across the 85 lung cancer cell lines (Figure 1A): in decreasing order of significance, these were 14q13.2 ($q = 0.0013$), 11p13 ($q = 0.015$), 1q21.2 ($q = 0.048$), 5p15.33 ($q = 0.085$), and 7p12.1 ($q = 0.19$). Amplifications of 1q21.2, 5p15.33, 7p12.1, and 14q13.2 have been previously reported in lung adenocarcinomas and revealed to harbor known lung cancer oncogenes (*ARNT*, *TERT*, *EGFR*, and *NKX2-1*, respectively), indicative of consistency between array platforms (5, 9). Although the amplicon associated with 11p13 has been previously reported and is thought to be a predictive marker in lung adenocarcinomas (7, 10), to our knowledge, the relevance to human lung cancer is not known.

High-level amplification of 11p13 was the second most significant event in our panel of NSCLC and SCLC cell lines ($q = 0.015277$), with the peak amplified region identified by GISTIC spanning an approximately 4-Mb interval (32,126,542–37,251,933 Mb) that contains 26 protein-coding genes (Figure 1B), none of which have been previously implicated in lung cancer. To identify candidate target genes, we next searched for concomitantly amplified and overexpressed genes within this interval by integrating parallel genetic and gene expression data for the cell lines. Of the 26 genes in the peak region, only *TRAF6* (36,467,531–36,488,372 bp) expression was positively and significantly associated with gene amplification (adjusted $P = 0.01$) (Figure 1C, Supplemental Figure 1, and Supplemental Table 1; supplemental material available online with this article; doi:10.1172/JCI58818DS1). Consistent with *TRAF6* mRNA overexpression (Supplemental Figure 1), TRAF6 protein was approximately 2-fold higher in lung cell lines with 11p13 amplification ($n = 5$) than in samples with diploid 11p13 ($n = 4$) (Figure 1D).

In total, *TRAF6* amplification was observed in 17 of 85 (20%) of the lung cancer cell lines, with the vast majority (88%) belonging to the NSCLC subtype (Table 1 and Supplemental Table 2). To confirm the cell line findings, we expanded our analysis to a panel of 261 clinical NSCLC tumor samples. Of these tumors, 24 (9.2%) had a copy number increase of the *TRAF6* genomic locus (Table 1), highlighting its potential clinical relevance. Furthermore, examination of matched gene expression data for lung tumor samples revealed a significant association between copy number amplification and *TRAF6* mRNA overexpression ($P = 0.035$; Figure 1E), further validating our cell line findings (Supplemental Figure 1). Thus, our integrative genomic analyses identified *TRAF6* as the target of the 11p13 amplicon, underlining a putative oncogenic role for this gene in lung cancer development.

TRAF6 is a member of the TNF receptor–associated factor (TRAF) family of proteins and is an E3 ubiquitin ligase that catalyzes autologous synthesis of lysine 63–linked (K63-linked) polyubiquitin chains involved in downstream activation of NF-κB (11). Despite its prominent role in NF-κB activation, TRAF6 has not to our knowledge been directly associated with oncogenesis. To determine whether TRAF6 overexpression leads to malignant cellular transformation, we retrovirally expressed TRAF6 in nontransformed mouse fibroblasts (NIH3T3) and evaluated cell growth and colony formation. Overexpression of TRAF6 resulted in enhanced cell proliferation in serum-deprived conditions (Figure 2A), formation of anchorage-independent colonies in soft agar comparable in size to colonies transformed with a constitutively active version of RAS, vH-RAS ($P = 0.0047$; Figure 2, B and C), and adoption of a spindle morphology and refractility, consistent with a transformed phenotype and similar to that of vH-RAS–transformed cells (Figure 2C). Vector-transduced cells were not refractile and grew in monolayers, morphologically resembling parental cells (Figure 2C). TRAF6- or vector-expressing NIH3T3 cells were injected subcutaneously into NOD/SCID mice and monitored for tumor growth. TRAF6-expressing cells began to form tumors within 4 weeks ($P = 0.011$; Figure 2D), and after 35 days, 80% (9 of 11) of mice developed large tumors (Figure 2D). Of the mice injected with control cells, only 1 developed a palpable tumor after 8 weeks (Figure 2D). These results are suggestive of the oncogenic capabilities of TRAF6, including the capacity to malignantly transform cells and form tumors.

Individual TRAF6-expressing clones were isolated from soft agar and independently expanded in liquid culture for further analysis. We reevaluated 3 TRAF6 clones (designated C1, C2, and C3) for colony formation in soft agar; these exhibited increased colony-forming ability compared with parental TRAF6-expressing NIH3T3 cells (data not shown). Examination of the TRAF6 clones revealed a pronounced transformed phenotype, including increased refractility, spindle morphology, and multilayered growth (Figure 2E). All TRAF6 clones exhibited higher TRAF6 protein expression (~2-fold) than that of the parental TRAF6-expressing cells (Figure 2F), and TRAF6 protein positively correlated with enhanced colony formation ($r^2 = 0.8032$; $P = 0.1$; Figure 2G). Consistent with a more aggressive transformed phenotype, tumor size was increased and latency reduced in the TRAF6 clones, approaching that of vH-RAS–induced tumors (Figure 2, H and I). Therefore, a higher level of TRAF6 expression was associated with malignant transformation.

Table 1
Incidence of 11p13 amplifications in human lung cancer

Material	11p13 amplification (*n*)	Total (*n*)	Incidence (%)
Lung tumors	24	261	9.2
Lung cell lines	17	85	20.0

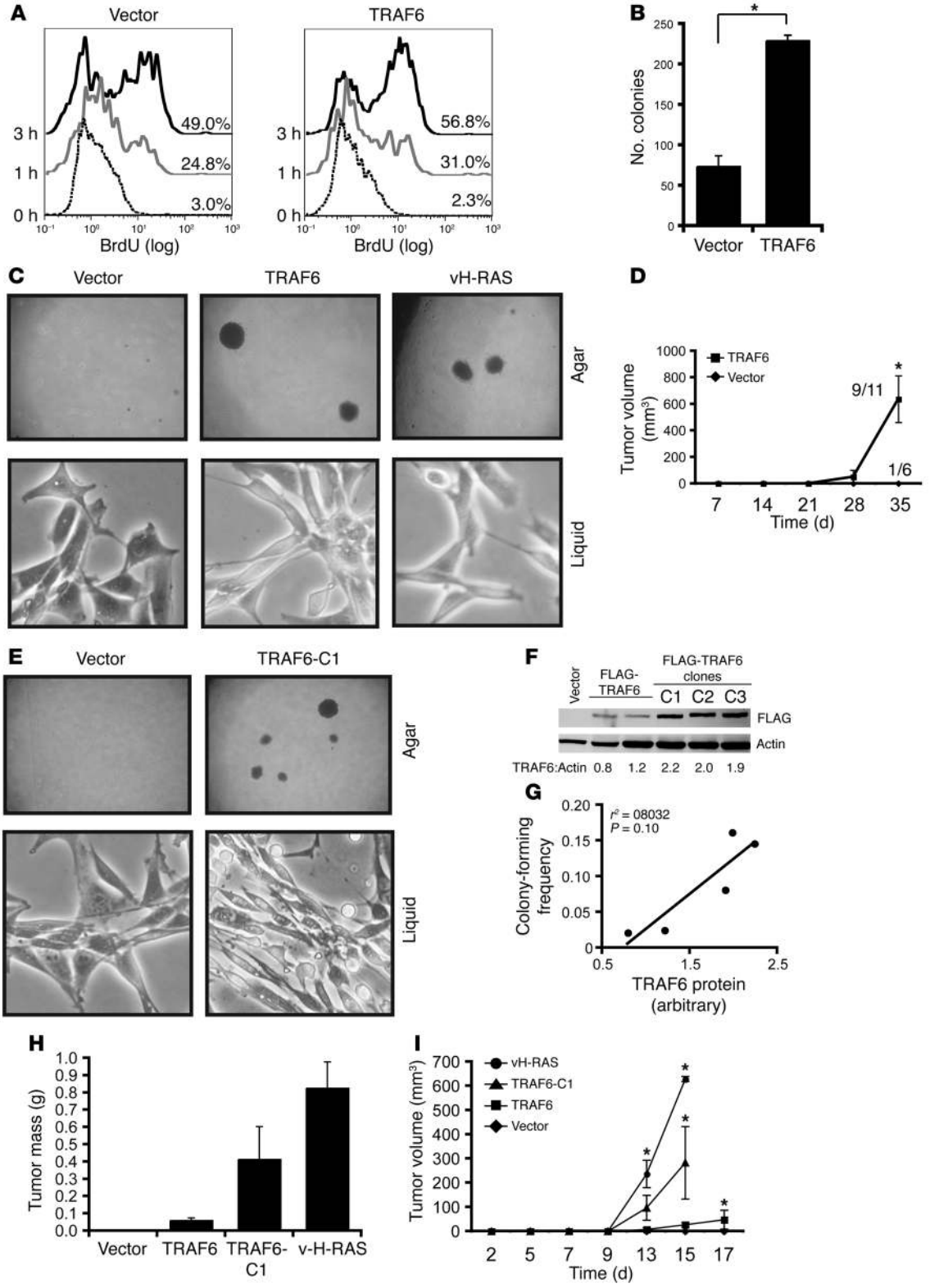
A
Vector
TRAF6
3 h
1 h
0 h
49.0%
24.8%
3.0%
56.8%
31.0%
2.3%
BrdU (log)
B
No. colonies
Vector
TRAF6
C
Vector
TRAF6
vH-RAS
Agar
Liquid
D
TRAF6
Vector
Tumor volume (mm³)
9/11
1/6
Time (d)
E
Vector
TRAF6-C1
Agar
Liquid
F
Vector
FLAG-TRAF6
FLAG-TRAF6 clones
C1 C2 C3
FLAG
Actin
TRAF6:Actin 0.8 1.2 2.2 2.0 1.9
G
r² = 08032
P = 0.10
Colony-forming frequency
TRAF6 protein (arbitrary)
H
Tumor mass (g)
Vector
TRAF6
TRAF6-C1
v-H-RAS
I
vH-RAS
TRAF6-C1
TRAF6
Vector
Tumor volume (mm³)
Time (d)

Figure 2
TRAF6 overexpression causes malignant phenotype. (**A**–**C**) NIH3T3 cells transduced with vector (MSCVpac) or FLAG-tagged TRAF6 were selected in puromycin and assessed (**A**) for growth in 2% serum by BrdU incorporation and (**B**) for colony formation in 0.3% soft agar (1×10^4 cells plated). (**C**) Morphology of vector- and TRAF6-expressing NIH3T3 cells is shown in agar and in liquid culture. Original magnification, ×20 (agar); ×40 (liquid). (**D**) NIH3T3 cells transduced with vector or TRAF6 were subcutaneously injected (2.5×10^5 cells/flank) into NOD/SCID mice and assessed for tumor formation by measuring tumor volume. (**E**) Individual colonies formed by TRAF6-expressing NIH3T3 cells were extracted from soft agar, expanded in liquid culture, and reanalyzed for soft agar colony formation. Representative cells are shown. Original magnification, ×20 (agar); ×40 (liquid). (**F**) 3 TRAF6 clones (C1–C3), along with 2 independently created parental TRAF6 cells and vector-expressing cells, were evaluated for FLAG-TRAF6 expression by IB (anti-FLAG). Densitometric values for FLAG-TRAF6 protein relative to actin are shown below. (**G**) Colony-forming frequency (no. colonies/1×10^3 cells plated) is shown relative to expression of FLAG-TRAF6 for TRAF6 clones ($n = 3$) and parental TRAF6 cells ($n = 2$). (**H** and **I**) NIH3T3 cells transduced with vector, TRAF6, vH-RAS, or TRAF6 clone C1 were subcutaneously injected (2.5×10^5 cells/flank) into NOD/SCID mice and assessed for tumor formation by measuring (**H**) tumor mass at day 15 and (**I**) tumor volume. *$P < 0.05$.

To investigate the role of TRAF6 in cell survival and oncogenesis in human lung cancer, we used RNA interference (RNAi) to knock down the expression of TRAF6. We chose 6 human lung cancer lines based on 11p13 amplification, *KRAS* mutation status, and a *RAS* gene expression signature (ref. 12 and Supplemental Table 3). To reduce expression in H1395, H460, and HCC95 cell lines, 3 independent retroviral shRNAs targeting discrete regions of *TRAF6* (shT6) were used, resulting in an approximately 50% knockdown of *TRAF6* mRNA (Supplemental Figure 2).

RNAi-mediated knockdown of TRAF6 significantly decreased the cell growth of adenocarcinoma lung lines HCC95 and SK-MES-1, which have *TRAF6* amplification ($P = 0.00036$ and $P = 0.025$, respectively, at day 8; Figure 3A). TRAF6 depletion also inhibited — albeit not as effectively — growth and viability of cell lines H460 and H2347, without an amplified *TRAF6* locus but with a *KRAS* mutation ($P = 0.01$ and $P = 0.034$, respectively; Figure 3A). Similarly, depletion of TRAF6 in lines H1395 and H520, without a *TRAF6* amplification (low TRAF6 protein) or *KRAS* mutation, had no or moderate effect on cell growth ($P = 0.14$ and $P = 0.006$, respectively; Figure 3A). Depletion of TRAF6 also led to a significant decrease in anchorage-independent colony growth of HCC95 ($P = 1.3 \times 10^{-7}$), SK-MES-1 ($P = 0.0009$), H2347 ($P = 4.9 \times 10^{-5}$), H460 ($P = 2.2 \times 10^{-5}$), and H520 ($P = 4.2 \times 10^{-5}$) cells, but not of H1395 cells ($P = 0.25$; Figure 3, B and C). In support of the growth and colony-forming data, cell viability was significantly reduced in H460 and HCC95 cells after TRAF6 depletion (P = 0.029; Figure 3D). Given that we observed a TRAF6-dependent cell line that did not have *KRAS* mutation or *TRAF6* amplification (H520), it is possible that other driver mutations affecting RAS or NF-κB signaling occur in this cell line, making it sensitive to TRAF6 inhibition.

We next subcutaneously injected shT6- or vector-expressing lung cancer cells into NOD/SCID mice and monitored tumor growth. Consistent with the colony formation observations, tumor-forming ability was significantly impaired after TRAF6 depletion in lines H460 and HCC95 ($P = 0.001$ and $P = 0.013$, respectively); however, TRAF6 knockdown in H1395 cells did not have an effect on tumor formation (Figure 3, E–G). Overall, these observations demonstrate an oncogenic role of TRAF6 in human lung cancers and suggest that cells with 11p13 amplifications or *KRAS* mutations may depend on TRAF6 for cell viability and tumor formation.

To determine whether other genes within the 11p13 amplicon are also relevant to the pathogenesis of human lung cancers, we evaluated 3 genes with *P* values approaching significance in our panel of lung cancers (see Supplemental Table 1). Inhibition of *COMMD9* ($P = 0.3$), *CD44* ($P = 0.031$), and *TCP11L1* ($P = 0.011$) did not suppress colony formation as effectively as did *TRAF6* inhibition ($P = 0.00021$; Supplemental Figure 3), which suggests that *TRAF6* is the critical gene within the 11p13 amplicon.

Somatic activating mutations of *KRAS* are the most frequent genetic events in NSCLCs (1). Despite the prominence of MAPK pathway activation by RAS (13, 14), NF-κB is also essential for *KRAS*-mediated lung cancers in mouse models (2, 15, 16). The importance of NF-κB is further supported by reports of constitutive NF-κB activation in more than 50% of human lung cancers (3). Despite high levels of NF-κB activation in human lung tumors and a critical role in RAS-mediated lung cancer formation in vivo, the mechanisms leading to constitutive NF-κB activation in human lung cancers remains unknown. Because TRAF6 is an upstream activator of NF-κB, we wanted to investigate whether TRAF6 is a key activator of NF-κB in human lung cancer. Therefore, 8 lung adenocarcinoma cell lines were evaluated for NF-κB activation. The lung lines with *TRAF6* amplification and overexpression displayed increased NF-κB activation, as determined by κB-site luciferase activity (11p13 amplification, 8.9 ± 5.9; no 11p13 amplification, 3.5 ± 1.5; $P = 0.1$), and by a shift toward nuclear translocation of the NF-κB subunit, p65 (Figure 4, A and B). Inhibition of TRAF6 in HCC95 (11p13 amplification) resulted in a significant decrease of NF-κB activation ($P = 0.0014$; Figure 4C). Inhibition of TRAF6 in H460 cells, which have a *KRAS* mutation, similarly resulted in a significant decrease of NF-κB activation ($P = 0.027$; Figure 4D). These findings suggest that increased TRAF6 expression is a potential cause of constitutive NF-κB activation in human lung cancers.

We observed that TRAF6 inhibition reduced NF-κB activation and tumor formation of lung cancer cells with *KRAS* mutations (Figures 3 and 4); therefore, we wanted to investigate whether TRAF6 is also an essential link in RAS-mediated tumorigenicity. To investigate a relationship between mutant *KRAS* and *TRAF6* amplifications, we examined an additional 705 human cancer cell lines. As expected, samples with *TRAF6* gain and/or amplification had significantly higher mRNA levels of this gene than did cell lines without *TRAF6* copy number increase ($P < 0.0001$). In this panel of cell lines, *KRAS* mutations were enriched in samples with *TRAF6* amplifications (17%; 21 of 125) compared with samples diploid at 11p13 (11%; 68 of 632; $P = 0.043$, Fisher exact test; Table 2). Therefore, there was an association between *KRAS* mutation and *TRAF6* copy number change, further supporting the interaction between these genes during tumorigenesis.

E3 ligase–mediated autoubiquitination is a measure of TRAF6 activation. To determine whether RAS also activates TRAF6, we overexpressed constitutively active *KRAS* or vH-RAS, subjected TRAF6 to IP, and measured TRAF6 polyubiquitination. As shown in Figure 5A, expression of *KRAS* activating mutant (V12) or vH-RAS resulted in autoubiquitination of TRAF6; however, an inactive *KRAS* mutant (N17) did not, validating previous findings (17). Inhibition of mutant *KRAS* abrogated TRAF6 autoubiquitination in an NSCLC cell line with mutant *KRAS* (Figure 5B).

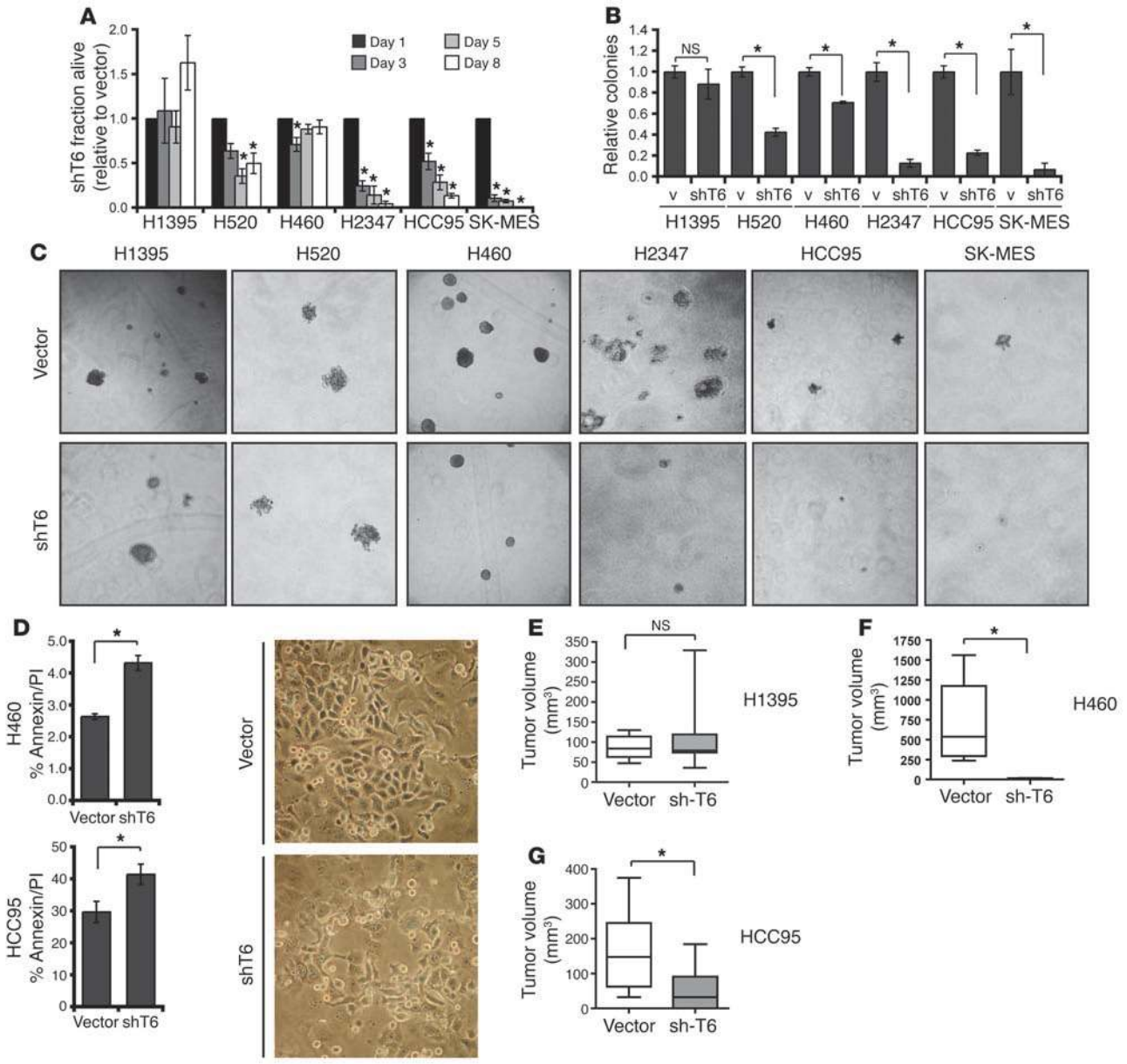

Figure 3

Inhibition of TRAF6 impairs growth and tumor formation of lung cancer cells. (**A**) Growth curves of cell lines with TRAF6 inhibition (shT6) is shown relative to vector-expressing (pLKO.1 control) cells. (**B** and **C**) Soft agar colony formation for the indicated cell lines after TRAF6 inhibition. Original magnification, ×20. (**D**) Cell lines H460 and HCC95 were transduced with virus encoding shT6. After TRAF6 inhibition, cell survival was evaluated by flow cytometry for Annexin V expression. HCC95 cells transduced with vector or shT6 were also cultured in liquid media, and morphological assessment confirmed that shT6-expressing cells exhibited features of increased cell death, such as cell detachment and shrinkage and membrane blebbing. Original magnification, ×40. (**E**–**G**) Cell lines H1395 (**E**), H460 (**F**), and HCC95 (**G**), transduced with vector (pLKO.1-control) or shT6, were subcutaneously injected into NOD/SCID mice. Tumor volume is shown at the experimental endpoint. *$P < 0.05$.

These findings suggest that TRAF6 activation may occur in human lung cancer through active *KRAS*, as previously proposed in other cellular contexts (17).

RAS dependence on TRAF6 was evaluated by overexpressing vH-RAS, a constitutively active version of RAS (18), in *Traf6*$^{-/-}$ mouse embryonic fibroblasts (MEFs; Figure 5C) or in NIH3T3 cells coexpressing a dominant-negative TRAF6 (T6DN) construct. In contrast to *Traf6*$^{+/+}$ cells (Figure 5, D and F), vH-RAS–mediated anchorage-independent growth was completely abrogated in *Traf6*$^{-/-}$ cells (Figure 5, D and F) and significantly reduced in NIH3T3 coexpressing T6DN (Figure 5, E and F; $P = 0.04$). Similarly, the ability of vH-RAS–expressing cells to form tumors was completely abolished in the absence of TRAF6 (Figure 5, G and H) and was significantly impaired when TRAF6 was blocked with T6DN ($P = 0.053$; Figure 5I). These findings suggest that RAS-mediated anchorage-independent colony growth, tumor formation, and NF-κB activation are dependent on TRAF6. Given the prominent role of TRAF6 in human lung cancers, we hypothesized that the

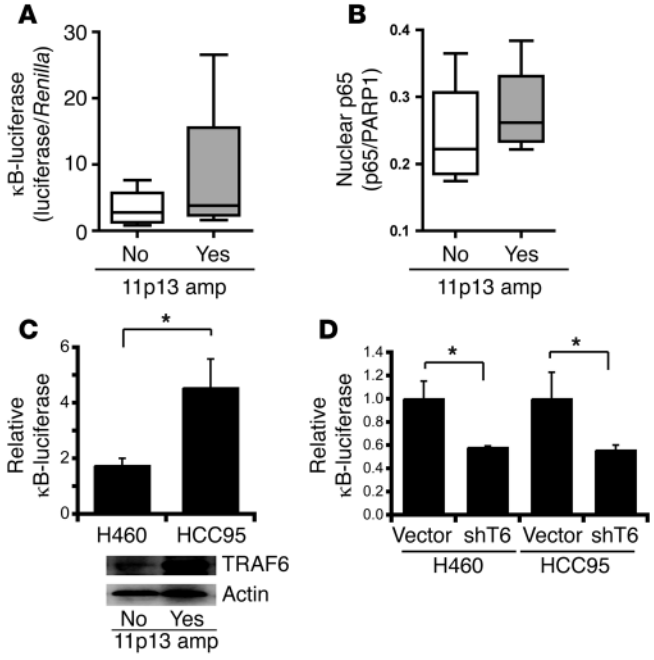

Figure 4
TRAF6 is upstream of NF-κB in human lung cancer cells. (**A**) NF-κB activity was measured by κB-site luciferase assays in human lung cancer cells with (HCC95, H526, H2171, HTB58) and without (H2170, H2347, H520, HTB117) amplification of the *TRAF6* locus (11p13). (**B**) Nuclear NF-κB (p65) was IB in nuclear extracts from 7 human lung cancer cell lines with (H2170, H2347, H520) or without (H2170, H2347, H520, HTB117) amplification at the *TRAF6* locus (11p13). (**C**) H460 (diploid at 11p13) and HCC95 (amplification of 11p13) were evaluated for κB-site luciferase activity and for TRAF6 protein expression. (**D**) NF-κB activity was measured by κB-site luciferase assays after *TRAF6* inhibition. *$P < 0.05$.

TRAF6 locus is also frequently amplified in other human cancers. By aCGH, we identified frequent amplification of the *TRAF6* locus in a panel of 124 additional human cancer cell lines (Table 3). In addition, we investigated whether *TRAF6* amplifications exist in a broader analysis of human cancer cell lines. In total, 757 cancer cell lines were analyzed, of which 126 (16.6%) displayed *TRAF6* copy number gain and/or amplification. In a subset of 705 of these cell lines that had matching expression data, samples with *TRAF6* gain and/or amplification had significantly higher mRNA levels of this gene compared with cell lines without *TRAF6* copy number increase ($P < 0.0001$, Mann-Whitney *U* test), confirming the findings from the lung cancer analyses. Beroukhim et al. also reported amplification of the *TRAF6* locus as a somatic and frequent event in several human cancer types (19). In our analysis, breast cancers exhibited amplification of 11p13 in approximately 30% of samples. In these cell lines, *TRAF6* mRNA overexpression also correlated with amplification of 11p13 (Supplemental Figure 4). Overexpression of T6DN in MCF7, a breast cell line with high levels of *TRAF6* expression, abrogated anchorage-independent colony growth in vitro ($P = 0.023$; Supplemental Figure 4). In contrast, SKBR3, a breast cell line with lower levels of *TRAF6*, were not sensitive to *TRAF6* inhibition ($P = 0.32$; Supplemental Figure 4).

Discussion

TRAF6 functions as a molecular bridge and key activator of NF-κB. Here, we identified *TRAF6* as one of the amplified candidate oncogenes on chromosome 11p13 in lung cancer cells. Overexpression of TRAF6 resulted in malignant transformation of fibroblasts and tumor formation, whereas knockdown of TRAF6 suppressed human lung cancer growth and tumor formation. Our finding that deletion of TRAF6 by RNAi suppressed RAS-mediated tumor formation may have important implications in human lung cancers. *KRAS* is one of the most frequently mutated oncogenes in lung cancers; however, effective therapies to inhibit RAS do not exist (1). Therefore, identification of TRAF6 as a downstream effector of RAS tumorigenesis may provide an alternative target for therapeutic intervention.

KRAS has been well documented as an activator of the NF-κB pathway in lung cancer; however, the components linking *KRAS* to NF-κB are not clear. The signaling adaptor p62 (also known as sequestosome) was recently identified as a critical target of RAS-induced mouse lung adenocarcinomas and NF-κB activation and as necessary for survival of human lung adenocarcinomas (17). It was shown that p62 activates IκB kinase (IKK), the central component of NF-κB, through TRAF6 autoubiquitination. Despite the requirement of NF-κB in tumor development and RAS signaling, the essential role of NF-κB in *KRAS*-driven lung adenocarcinomas was not revealed until recently. Genetic inhibition of NF-κB showed that NF-κB is critical to the development of mouse lung adenocarcinomas driven by the *KRAS* G12D mutation (2). In an independent finding, a systematic RNAi screen revealed that *KRAS*-driven lung cancers require TBK1 and c-REL, 2 components of the NF-κB signaling cascade (16). Taken together, these observations suggest that the role of TRAF6 in lung cancer may be as a mediator of NF-κB activation.

TRAF6 activates the NF-κB pathway by sequential steps, including K63-linked autoubiquitination at N-terminal lysines, followed by ubiquitination of TAK1 and IKK-γ (also known as NEMO). Interestingly, the TRAF6 deubiquitinating enzyme cylindromatosis (CYLD) is found mutated in cylindromatosis malignancies and multiple myeloma (20–22). These mutations result in an inability of CYLD to deubiquitinate TRAF6 (23). Consistent with the role of TRAF6 in lung cancer, downregulation of CYLD expression is associated with the development of lung adenocarcinomas (24). Although autoubiquitination is important for full TRAF6 activation, some evidence suggests that TRAF6 can activate NF-κB and MAPK in response to IL-1 and RANKL independent of its autoubiquitination ability (25).

In our recent study, overexpression of TRAF6 in primary mouse marrow cells results in a myelodysplastic syndrome that develops into a fatal acute myeloid leukemia (26). TRAF6 protein levels are also higher in myelodysplastic syndrome patients (26). Beroukhim et al. also reported amplification of the *TRAF6* locus as a somatic and frequent event in several human cancer types (19). Despite these findings, the precise role of TRAF proteins in cancer has not been extensively investigated. Empirical differences in TRAF protein expression in human cancer have been reported (27). TRAF2 and TRAF6, which share many structural and functional similarities, exhibit the highest and most consistent expression in human cancer cell lines (27). TRAF2 has previously been implicated in pancreatic cancers. It is overexpressed in pancreatic tumors and cell lines, activates NF-κB, promotes invasiveness, and protects tumor cells from CD95-mediated apoptosis (28). Interestingly, amplification of the *TRAF2* locus (9q34.3; 138,900,786–138,940,887 bp) was another common event in our set of lung cancers (~40% incidence;

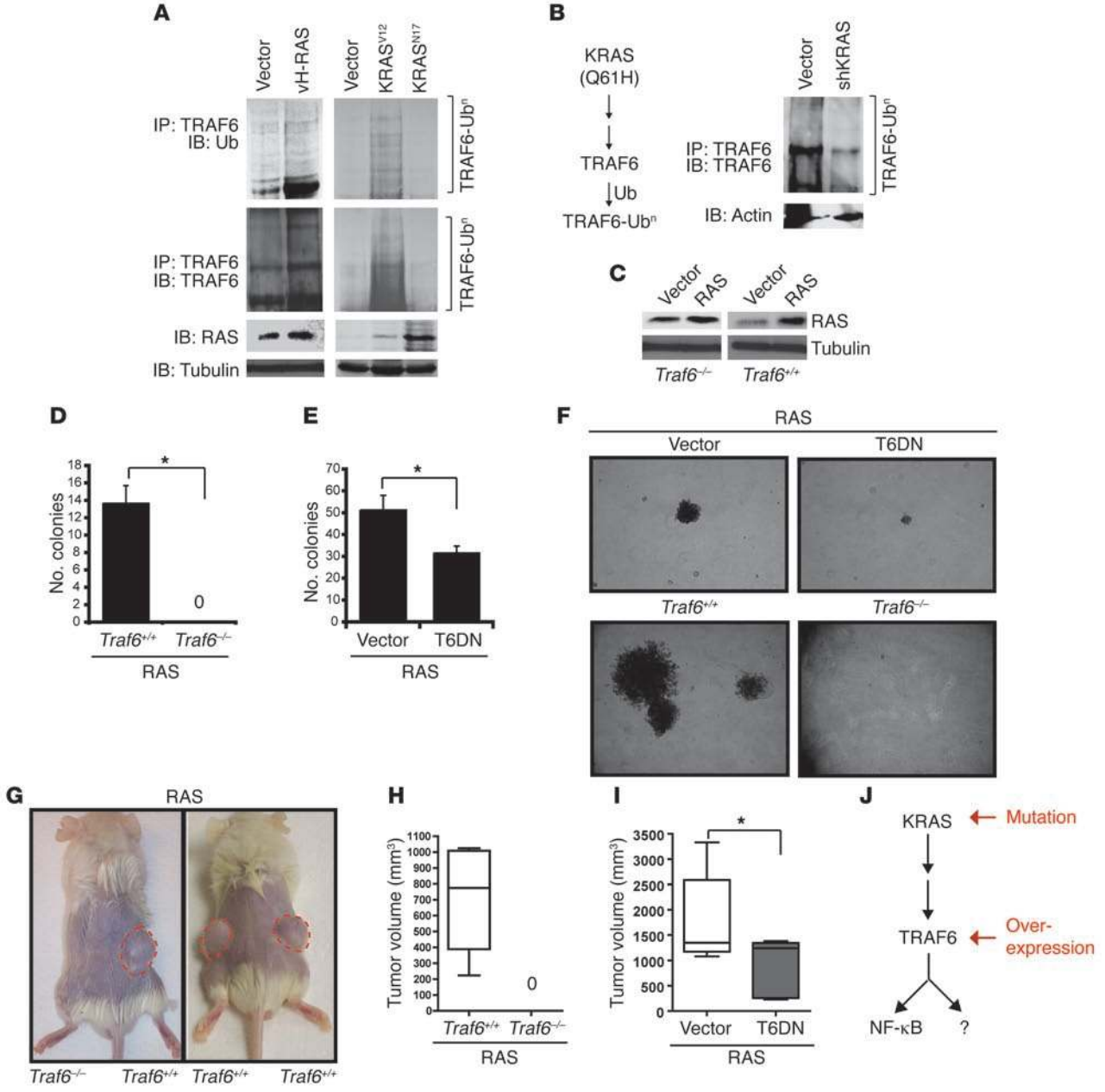

Figure 5

TRAF6 is necessary for RAS-mediated oncogenesis. (**A**) Extracts from HEK293 cells transfected with the indicated vectors were IP with an anti-TRAF6 antibody, then IB for polyubiquitination with ubiquitin or TRAF6 antibodies. RAS and tubulin were determined by IB on the pre-IP lysates. (**B**) Extracts from H460 cells (*KRAS* mutation) transduced with the indicated shRNA vectors were IP with an anti-TRAF6 antibody, then IB with anti-TRAF6 antibodies. Actin was IB on the pre-IP lysates. A proposed model of *KRAS*-mediated activation of TRAF6 in lung cancer is also shown. (**C**) *Traf6*$^{-/-}$ or *Traf6*$^{+/+}$ MEFs were transduced with a retroviral vector encoding vH-RAS (MSCVpac) and IB for RAS. (**D**) Soft agar colony formation for vH-RAS–expressing *Traf6*$^{-/-}$ or *Traf6*$^{+/+}$ MEFs (1×10^4 cells plated). (**E**) Soft agar colony formation for vH-RAS–expressing NIH3T3 cells transduced with T6DN or vector control (MIY). (**F**) Representative colonies from **D** and **E**. Original magnification, ×20. (**G** and **H**) vH-RAS–expressing *Traf6*$^{-/-}$ or *Traf6*$^{+/+}$ MEFs were subcutaneously injected into NOD/SCID mice. (**G**) Representative tumors (red outline) on the dorsa. (**H**) Tumor volume at the experimental endpoint. (**I**) vH-RAS–expressing NIH3T3 cells transduced with T6DN or vector control were subcutaneously injected into NOD/SCID mice. Tumor volume is shown at the experimental endpoint. (**J**) Model of TRAF6-sensitive lung cancers. For TRAF6 inhibition–sensitive lung cancers, TRAF6 inhibition reduced proliferation, anchorage-independent growth, tumor formation, and NF-κB activation. *$P < 0.05$.

data not shown), and inhibition of TRAF2 suppresses growth and radiosensitizes lung cancer (29). Amplification and overexpression of TRAF2 may constitute a mechanism of NF-κB activation and tumor formation in lung cancers similar to that of *TRAF6*.

We demonstrate that *TRAF6* is one of the amplified candidate oncogenes on chromosome 11p13 and likely contributes to the pathogenesis of human lung cancer. Although other candidate genes may reside on 11p13, inhibition of TRAF6 reduced NF-κB

Table 2
Incidence of *KRAS* mutations and *TRAF6* amplifications

	***TRAF6* amplification**	**No *TRAF6* amplification**
***KRAS* mutation**	21	68
No *KRAS* mutation	104	564

Incidence data show total *n* for each pairing. $P = 0.0428$, 1-tailed Fisher exact test.

activation and suppressed tumor growth of human lung cancers harboring 11p13 amplifications, which suggests that it is important for tumorigenesis. Not only were lung cancer samples with 11p13 amplifications dependent on TRAF6 for their malignant state, but lung cancer samples with *KRAS* mutations (but normal TRAF6 expression) were sensitive to TRAF6 inhibition. Therefore, *TRAF6* amplification in lung tumors — with or without *RAS* mutations — may explain constitutive NF-κB activation in a majority of lung cancers. We also reported, for the first time to our knowledge, that overexpression of TRAF6 led to malignant transformation and tumor formation, implicating *TRAF6* as a bona fide oncogene.

Methods

Sample collection, cell lines, and plasmids. Cancer-derived cell lines were collected as previously described (7). All lung cell lines used in this study and their characteristics are listed in Supplemental Table 2. Mutation data for the lung cancer cell lines were obtained from the Sanger Institute's Cancer Cell Line Project website (http://www.sanger.ac.uk/genetics/CGP/CellLines/). 261 formalin-fixed, paraffin-embedded, or fresh-frozen tissue tumor specimens were collected from Vancouver General Hospital and Princess Margaret Hospital following approval by the Institutional Research Ethics Boards. Hematoxylin and eosin–stained sections for each sample were graded by a lung pathologist for use in selecting regions for manual microdissection to ensure greater than 70% tumor cell content. DNA for cell lines and tumors was isolated using standard procedures, with proteinase K digestion followed by phenolchloroform extraction as previously described (7). Spontaneously immortalized *Traf6*$^{-/-}$ and *Traf6*$^{+/+}$ MEFs were provided by T. Mak and W.C. Yeh (University of Toronto, Toronto, Ontario, Canada). H1395 and H520 are diploid at the *TRAF6* locus (11p13), contain wild-type *KRAS* alleles, and are not reported to have a RAS gene expression signature. H460 and H2347 are diploid at the *TRAF6* locus and contain a mutant *KRAS* (Q61H) allele, but are reported to have a RAS signature. HCC95 and SK-MES-1 contain wild-type *KRAS* alleles, but harbor an amplification of the *TRAF6* locus. Although there are no reports on HCC95 gene expression, SK-MES-1 are reported to have a RAS signature. Flag-tagged TRAF6 and T6DN cDNAs were provided by Tularik and cloned into MSCVpac and MSCV-IRES-YFP (MIY). vH-RAS (MSCVpac) was a gift from T. Gilmore (Boston University, Boston, Massachusetts, USA). cDNAs of *KRAS* activating and inactive *KRAS* mutants (V12 and N17, respectively) were provided by R. Kay (British Columbia Cancer Research Centre, Vancouver, British Columbia, Canada). The pLKO.1 (OpenBiosystems) construct was used to generate shRandom, shT6, shKRAS, shCD44, shTCP11L1, and shCOMMD9. 4 independent pLKO.1-shT6 constructs were obtained: shT6-1 (TRCN0000007348), shT6-2 (TRCN0000007349), shT6-3 (TRCN0000007351), and shT6-4 (TRCN0000007352). Single pLKO.1-sh constructs were obtained for shKRAS (TRCN0000034384), shCD44 (TRCN0000057563), shTCP11L1 (TRCN0000200624), and shCOMMD9 (V2LHS254179).

Whole-genome tiling path aCGH and data analysis. DNA copy number profiles were generated for each sample using whole-genome tiling path aCGH (30). Details of the genomic array, DNA extraction, labeling and hybridization, image analysis, and normalization have been described previously (30, 31). SIGMA^2 software was used to visualize all data as $\log_2$ ratio plots (32). All probes were mapped to March 2006 (hg18) genomic coordinates. All raw array data files are available through the System for Integrative Genomic Microarray Analysis (SIGMA; http://sigma.bccrc.ca) (32) and have been deposited in GEO (accession no. GSE31800). aCGH-Smooth (33) was used to smooth ratio values and identify copy number breakpoints for each sample as previously described (7). The resulting segments and ratio values were then analyzed using the GISTIC method (8) to determine regions of significant amplification and deletion across the samples. Analysis was performed using Gene Pattern software (www.broad.mit.edu/cancer/software/genepattern/) with default settings. aCGH-Smooth segments less than 2 probes in length were removed prior to analysis. In addition, known regions of copy number variation in the normal population (34) were removed during the analysis. Segments displaying an average $\log_2$ ratio greater than 0.8 for a region were considered to have high-level amplification (7), and thus used as the GISTIC $\log_2$ ratio threshold. The frequency of *TRAF6* copy number alteration in tumors and cell lines was performed using aCGH-Smooth ratios, as previously described (35). Sanger Institute's Cancer Cell Line Project (http://www.sanger.ac.uk/genetics/CGP/CellLines/) was used to investigate whether *TRAF6* amplifications exist in human cancer cell lines.

Gene expression analysis. Gene expression data for the lung cancer cell lines were generated using the Affymetrix Gene Chips HG-U133A and HG-U133B and downloaded from the Gene Expression Omnibus (accession no. GSE4824) (36). Fresh-frozen lung tumors were obtained from Vancouver General Hospital as described above. Microdissection of tumor cells was performed, and total RNA was isolated using RNeasy Mini Kits (Qiagen Inc.). Samples were labeled and hybridized to a custom Affymetrix microarray, containing 43,737 probes mapping to approximately 23,000 unique genes, according to the manufacture's protocols (Affymetrix Inc.) All data were normalized using the Robust Multichip Average algorithm in *R* (37). Of the lung tumor cohort, only samples with sufficient material for RNA isolation were selected for expression analysis. The Director's Challenge Consortium for the Molecular Classification of Lung Adenocarcinoma was also used to analyze *TRAF6* gene expression (38).

Integration of genomic and gene expression data. Gene expression probes were mapped to March 2006 (hg18) genomic coordinates, and those within the peak 11p13 region identified by GISTIC were determined. If multiple probes were present for a gene, the one with the maximum intensity across all samples was used. To integrate gene expression with copy number data, we first separated samples based on their copy number status as previ-

Table 3
Incidence of 11p13 amplifications in human cancer cell lines

Cancer type	**11p13 amplification (*n*)**	**Total (*n*)**	**Incidence (%)**
Blood	2	6	33
Bone	1	2	50
Brain	1	5	20
Breast	10	35	29
Cervix	3	8	38
Colon	2	8	25
Kidney	3	8	38
Lymphoid	1	9	11
Ovary	2	7	29
Pancreas	7	20	35
Skin	3	10	30
Oral	3	6	50

ously described (39). Gene expression data were then compared between amplified and neutral copy number groups for each gene using the Mann-Whitney *U* test to identify those that were overexpressed in the amplified samples with a *P* value less than 0.05. As the direction of gene expression difference was predicted to match the direction of copy number difference, 1-tailed *P* values were calculated. A Bonferroni multiple-comparison testing correction was applied based on the total number of gene expression probes analyzed for the region. Probes with an adjusted *P* value of 0.05 or less were considered significant.

Lentiviral infections. For Rev-dependent lentivirus, HEK293T cells were contransfected with pLKO.1sh, RRE, VSV-G, and REV constructs. Virus was harvested and used to infect human lung cancer cell lines. Transduced cell lines were selected in puromycin.

Tumor and soft agar colony-forming studies. Retrovirally transduced NIH3T3, H1395, H460, HC995, or MEF cells were selected in puromycin for 2 weeks. For colony-forming assays, 1×10^3 to 1×10^4 cells were plated in 10% FBS in DMEM containing 0.3% agar and scored for colonies after approximately 2 weeks, according to published protocol (40). For clones, individual colonies were removed with a 1-ml pipet and transferred to 10% FBS in DMEM in 12-well plates. Cells were allowed to adhere and expand prior to reanalysis. Experimental approaches for tumor studies have been published elsewhere (41). Nonobese diabetic/severe combined immunodeficient mice were obtained from the Animal Resource Centre of the British Columbia Cancer Research Centre. For tumor implantation, NIH3T3 (2.5×10^5), H460 (1.5×10^5), H1395 (2.5×10^6), or HCC95 (1×10^6) cells were injected subcutaneously into the dorsa of mice. Tumor length and width were determined using calipers, and tumor volume was calculated as $(l \times w^2) \times 0.5$. For each time point, tumor data are presented as the mean tumor volume ± SEM for the indicated mice.

Western blot analysis. Cultured cells were lysed and analyzed by SDS-PAGE and IB with the following antibodies: TRAF6 (sc-7221; Santa Cruz), Tubulin (T-9026; Sigma-Aldrich), actin (sc-1615; Santa Cruz), FLAG (M5; Sigma), RAS (Zymed Laboratories), and ubiquitin (sc-8017; Santa Cruz). IP was performed with anti-TRAF6 antibody (sc-7221; Santa Cruz). Protein expression was quantitated by densitometry.

IP. For RAS overexpression, HEK293 cells were transfected with 4 μg vH-RAS (G12V), *KRAS* (G12D or N17), or vector control for 2 days. For RAS knockdown, H460 cells were infected with pLKO.1 (control vector) or shKRAS and then selected with puromycin for 10 days. HEK293 or H460 cells were lysed in 50 mM Tris-HCl (pH 7.6), 50 mM NaCl, 1 mM EDTA, 1% Triton-X, and protease inhibitor cocktail. TRAF6 or FLAG antibody (2 μg) was added to cell lysates (10 mg) for 3 hours at 4°C and captured by the addition of protein A or G beads for an additional 12 hours at 4°C. The immune complexes were washed 3 times with lysis buffer, followed by the addition of SDS sample buffer. The bound proteins were separated by SDS-polyacrylamide gel electrophoresis, transferred to nitrocellulose membranes, and analyzed by IB for ubiquitin and TRAF6.

Apoptosis analysis. Approximately 1×10^5 cells were washed in PBS and resuspended in Annexin V–binding buffer (10 mM HEPES; 140 mM NaCl; 2.5 mM $CaCl_2$; pH 7.4) and Annexin V–conjugated antibody (diluted 1:20). After a 15-minute incubation, an additional 500 μl Annexin V–binding buffer was added, and cells were analyzed by flow cytometry.

Proliferation assay. NIH3T3 cells transduced with vector or TRAF6 were starved overnight in media containing 2% serum, then pulsed with 10 μM BrdU for 0, 1, and 3 hours. As described previously (42), cells were harvested, fixed with 70% ethanol, and analyzed with an anti-BrdU–FITC antibody by flow cytometry.

NF-κB activation assays. For the NF-κB luciferase assays, 300 ng of a κB site-containing luciferase reporter plasmid and 10 ng of thymidine kinase–driven *Renilla* luciferase were cotransfected into HEK293 cells, NIH3T3 cells, or the indicated lung cancer lines (12-well format) using TransiT transfection reagent (Mirus). Values shown reflect luciferase values normalized to *Renilla*. For NF-κB translocation, 7 lung cancer cell lines (3 with amplification of 11p13; 4 diploid at 11p13) were cultured in RPM1 (10% FBS). The trypsized cells were washed once in ice-cold buffer A (10 mM HEPES-KOH, pH 7.8; 10 mM KCl; 1.5 mM $MgCl_2$). The supernatant was removed, and each pellet was resuspended in 375 μl buffer A containing protease inhibitor cocktail (Roche) and 0.5% NP-40 (Sigma-Aldrich). The lysate samples were allowed to sit on ice for 10 minutes before they were subjected to centrifugation at 12,000 *g* for 10 minutes at 4°C. The supernatant, which was the cytoplasmic fraction, was transferred to new mirocentrifuge tubes while each of the pellets was washed once with 375 μl buffer A. After centrifugation and removal of supernatant, each pellet was solubilized with 75 μl RIPA buffer containing protease inhibitor cocktail through incubation at 4°C for 20 minutes on a rotator. The nuclear lysate was centrifuged at maximum speed at 4°C for 15 minutes, and the supernatant was transferred to new microcentrifuge tubes as nuclear extracts. Nuclear extracts were then analyzed for NF-κB (anti-p65) and PARP1 (anti-Parp1) expression.

Preparation of cDNA and RT-PCR of mRNA. Total cellular RNA was extracted using TRIzol reagent (Invitrogen). The purified total RNA preparation was used as a template to generate first-strand cDNA synthesis using SuperScriptII (Invitrogen).

Statistics. Results are mean ± SEM. Statistical analyses were performed using Student's *t* test (1-tailed unless otherwise specified; $P < 0.05$ considered significant) and Mann-Whitney *U* test (gene expression data). Comparison of survival between different groups was done by the Kaplan-Meier test, and *P* value was calculated by the log-rank test. In box-and-whisker plots, bounds of the boxes denote 25th and 75th percentiles; lines within the boxes denote the 50th percentile (median); and whiskers denote range. GraphPad Prism (version 4; GraphPad) was used for statistical analysis.

Study approval. Studies using human material were approved by the University of British Columbia–British Columbia Cancer Agency Research Ethics Board (Vancouver, British Columbia, Canada). Written consent was obtained from all subjects. All animal protocols were approved by the Animal Care Committee of the University of British Columbia (Vancouver, British Columbia, Canada).

Acknowledgments

We thank Fred Wong and Denise McDougal for assistance with flow cytometry. We thank Sandy Sung and Nelson Wong for technical assistance. This research was supported by grants from the Canadian Institutes of Health Research (CIHR; MOP 97744 and MOP 89976 to A. Karsan; MOP 86731 and MOP 77903 to W. Lam) and the Canadian Cancer Society (017076 to A. Karsan; CCS20485 to W. Lam), the NCI Early Detection Research Network (5U01 CA84971-10 to A. Gazdar, W. Lam, and S. Lam), and the Canary Foundation (to W. Lam and A. Gazdar). D.T. Starczynowski was supported by postdoctoral fellowships from the CIHR and Michael Smith Foundation for Health Research (MSFHR). W. Lockwood and R. Chari were supported by a doctoral research award from the Natural Sciences and Engineering Research Council of Canada, CIHR, and MSFHR. A. Karsan is a Senior Scholar of the MSFHR.

Received for publication May 2, 2011, and accepted in revised form July 6, 2011.

Address correspondence to: Aly Karsan, British Columbia Cancer Agency Research Centre, 675 West 10th Avenue, Vancouver, British Columbia V5Z 1L3, Canada. Phone: 604.675.8033; Fax: 604.675.8049; E-mail: akarsan@bccrc.ca.

1. Herbst RS, Heymach JV, Lippman SM. Lung cancer. *N Engl J Med*. 2008;359(13):1367–1380.
2. Meylan E, et al. Requirement for NF-kappaB signalling in a mouse model of lung adenocarcinoma. *Nature*. 2009;462(7269):104–107.
3. Tang X, et al. Nuclear factor-kappaB (NF-kappaB) is frequently expressed in lung cancer and preneoplastic lesions. *Cancer*. 2006;107(11):2637–2646.
4. Yang Y, et al. A selective small molecule inhibitor of c-Met, PHA-665752, reverses lung premalignancy induced by mutant K-ras. *Mol Cancer Ther*. 2008; 7(4):952–960.
5. Weir BA, et al. Characterizing the cancer genome in lung adenocarcinoma. *Nature*. 2007; 450(7171):893–898.
6. Zhao X, et al. Homozygous deletions and chromosome amplifications in human lung carcinomas revealed by single nucleotide polymorphism array analysis. *Cancer Res*. 2005;65(13):5561–5570.
7. Lockwood WW, et al. DNA amplification is a ubiquitous mechanism of oncogene activation in lung and other cancers. *Oncogene*. 2008;27(33):4615–4624.
8. Beroukhim R, et al. Assessing the significance of chromosomal aberrations in cancer: methodology and application to glioma. *Proc Natl Acad Sci U S A*. 2007;104(50):20007–20012.
9. Kendall J, et al. Oncogenic cooperation and coamplification of developmental transcription factor genes in lung cancer. *Proc Natl Acad Sci U S A*. 2007; 104(42):16663–16668.
10. Sung JS, Park KH, Kim YH. Genomic alterations of chromosome region 11p as predictive marker by array comparative genomic hybridization in lung adenocarcinoma patients. *Cancer Genet Cytogenet*. 2010;198(1):27–34.
11. Chung JY, Park YC, Ye H, Wu H. All TRAFs are not created equal: common and distinct molecular mechanisms of TRAF-mediated signal transduction. *J Cell Sci*. 2002;115(Pt 4):679–688.
12. Loboda A, et al. A gene expression signature of RAS pathway dependence predicts response to PI3K and RAS pathway inhibitors and expands the population of RAS pathway activated tumors. *BMC Med Genomics*. 2010;3:26.
13. Shigematsu H, Gazdar AF. Somatic mutations of epidermal growth factor receptor signaling pathway in lung cancers. *Int J Cancer*. 2006;118(2):257–262.
14. Ji H, et al. Mutations in BRAF and KRAS converge on activation of the mitogen-activated protein kinase pathway in lung cancer mouse models. *Cancer Res*. 2007;67(10):4933–4939.
15. Basseres DS, Ebbs A, Levantini E, Baldwin AS. Requirement of the NF-kappaB subunit p65/RelA for K-Ras-induced lung tumorigenesis. *Cancer Res*. 2010;70(9):3537–3546.
16. Barbie DA, et al. Systematic RNA interference reveals that oncogenic KRAS-driven cancers require TBK1. *Nature*. 2009;462(7269):108–112.
17. Duran A, et al. The signaling adaptor p62 is an important NF-kappaB mediator in tumorigenesis. *Cancer Cell*. 2008;13(4):343–354.
18. Tabin CJ, Weinberg RA. Analysis of viral and somatic activations of the cHa-ras gene. *J Virol*. 1985; 53(1):260–265.
19. Beroukhim R, et al. The landscape of somatic copy-number alteration across human cancers. *Nature*. 2010;463(7283):899–905.
20. Bignell GR, et al. Identification of the familial cylindromatosis tumour-suppressor gene. *Nat Genet*. 2000;25(2):160–165.
21. Keats JJ, et al. Promiscuous mutations activate the noncanonical NF-kappaB pathway in multiple myeloma. *Cancer Cell*. 2007;12(2):131–144.
22. Annunziata CM, et al. Frequent engagement of the classical and alternative NF-kappaB pathways by diverse genetic abnormalities in multiple myeloma. *Cancer Cell*. 2007;12(2):115–130.
23. Trompouki E, Hatzivassiliou E, Tsichritzis T, Farmer H, Ashworth A, Mosialos G. CYLD is a deubiquitinating enzyme that negatively regulates NF-kappaB activation by TNFR family members. *Nature*. 2003;424(6950):793–796.
24. Zhong S, Fields CR, Su N, Pan YX, Robertson KD. Pharmacologic inhibition of epigenetic modifications, coupled with gene expression profiling, reveals novel targets of aberrant DNA methylation and histone deacetylation in lung cancer. *Oncogene*. 2007;26(18):2621–2634.
25. Walsh MC, Kim GK, Maurizio PL, Molnar EE, Choi Y. TRAF6 autoubiquitination-independent activation of the NFkappaB and MAPK pathways in response to IL-1 and RANKL. *PLoS One*. 2008; 3(12):e4064.
26. Starczynowski DT, et al. Identification of miR-145 and miR-146a as mediators of the 5q- syndrome phenotype. *Nat Med*. 2010;16(1):49–58.
27. Zapata JM, et al. TNFR-associated factor family protein expression in normal tissues and lymphoid malignancies. *J Immunol*. 2000;165(9):5084–5096.
28. Trauzold A, et al. CD95 and TRAF2 promote invasiveness of pancreatic cancer cells. *FASEB J*. 2005;19(6):620–622.
29. Zheng M, et al. Growth inhibition and radiosensitization of glioblastoma and lung cancer cells by small interfering RNA silencing of tumor necrosis factor receptor-associated factor 2. *Cancer Res*. 2008;68(18):7570–7578.
30. Ishkanian AS, et al. A tiling resolution DNA microarray with complete coverage of the human genome. *Nat Genet*. 2004;36(3):299–303.
31. Starczynowski DT, et al. High-resolution whole genome tiling path array CGH analysis of CD34+ cells from patients with low-risk myelodysplastic syndromes reveals cryptic copy number alterations and predicts overall and leukemia-free survival. *Blood*. 2008;112(8):3412–3424.
32. Chari R, et al. SIGMA2: a system for the integrative genomic multi–dimensional analysis of cancer genomes, epigenomes, and transcriptomes. *BMC Bioinformatics*. 2008;9:422.
33. Jong K, Marchiori E, Meijer G, Vaart AV, Ylstra B. Breakpoint identification and smoothing of array comparative genomic hybridization data. *Bioinformatics*. 2004;20(18):3636–3637.
34. Wong KK, et al. A comprehensive analysis of common copy-number variations in the human genome. *Am J Hum Genet*. 2007;80(1):91–104.
35. Coe BP, et al. Gain of a region on 7p22.3, containing MAD1L1, is the most frequent event in small-cell lung cancer cell lines. *Genes Chromosomes Cancer*. 2006;45(1):11–19.
36. Zhou BB, et al. Targeting ADAM-mediated ligand cleavage to inhibit HER3 and EGFR pathways in non-small cell lung cancer. *Cancer Cell*. 2006;10(1):39–50.
37. Irizarry RA, et al. Exploration, normalization, and summaries of high density oligonucleotide array probe level data. *Biostatistics*. 2003;4(2):249–264.
38. Shedden K, et al. Gene expression-based survival prediction in lung adenocarcinoma: a multi-site, blinded validation study. *Nat Med*. 2008; 14(8):822–827.
39. Campbell JM, et al. Integrative genomic and gene expression analysis of chromosome 7 identified novel oncogene loci in non-small cell lung cancer. *Genome*. 2008;51(12):1032–1039.
40. Gapuzan ME, Schmah O, Pollock AD, Hoffmann A, Gilmore TD. Immortalized fibroblasts from NF-kappaB RelA knockout mice show phenotypic heterogeneity and maintain increased sensitivity to tumor necrosis factor alpha after transformation by v-Ras. *Oncogene*. 2005;24(43):6574–6583.
41. Leong KG, et al. Jagged1-mediated Notch activation induces epithelial-to-mesenchymal transition through Slug-induced repression of E-cadherin. *J Exp Med*. 2007;204(12):2935–2948.
42. Leong KG, et al. Activated Notch4 inhibits angiogenesis: role of beta 1-integrin activation. *Mol Cell Biol*. 2002;22(8):2830–2841.